PS/HP/Note 99-01
AD Note 046
February 1999

ANALYSIS OF THE ELECTRON BEAM LINE FOR THE TEST OF THE RFQ DECELERATING SYSTEM FOR THE AD ANTIPROTON DECELERATOR

Alessandro Variola
CERN – PS Division – HP Group

INTRODUCTION

This study was developed within the framework of the realisation of a radio-frequency quadrupole (RFQ) decelerating system. It is meant for the antiproton beam on the AD machine end line, within the ASACUSA project [1]. In fact, the creation of a RFQ decelerating system would make it possible to reduce the antiproton beam energy and would entail a much higher current transmission factor than that obtained by means of a degrader foil. In Ref. [1] two methods were mentioned for the RFQ test: a) using the proton source in Aarhus (Denmark), which seems more costly; b) trying to scale the parameters of an electron beam so as to obtain a beam dynamically equivalent to the antiproton one. By dynamically equivalent beam it is meant an electron beam having the same beta as the antiproton beam (scaling kinetic energy), the same emittance and the same space charge contribution (scaling current). In this case the main stages to go through are the following:

1. Proof of principle, that is a test with any radio frequency device that has already been dynamically characterised with a proton beam allowing the measurement of the equivalent electron beam, so as to prove the validity of the principle. Basically, the idea is to use RFQ 2 [2].

2. Test on the decelerating RFQ designed for AD. In this case an electron beam having the same dynamic characteristics as the AD antiproton beam is needed at the RFQ entrance.

For these two stages to be implemented, three different electron beam configurations are required: one where the electron beam is equivalent to the proton one used in RFQ 2 in the accelerating direction; one enabling us, if possible, to make a test in the decelerating direction too; and one with the same characteristics as the AD antiproton beam. Let us analyse the main characteristics of the beams and their equivalents in these configurations and compute the most important dynamic parameters.

Table 1

1	Protons	Eq. Electrons
Case	RFQ 2 - accelerating	RFQ 2 - accelerating
Kinetic Energy	90 keV	49 eV
Emittance tot.unorm.	~174π mm mrad	~174π mm mrad
Current	100 – 200 mA	50 – 100 μA
Energy spread	Less than 5%	Less than 5%
α Twiss	2.0752	2.0752
β Twiss	0.10612 mm mrad^{-1}	0.10612 mm mrad^{-1}
β rel	0.01385	0.01385
γ rel	1.00009	1.00009

$$\beta_R = \left[1 - \left(1+\frac{T}{E_0}\right)^{-2}\right]^{1/2} = 0.0138475 \quad ; \quad \gamma_R = \frac{1}{\sqrt{1-\beta^2}} = 1.0000959$$

$$\beta_R \gamma_R = 0.0138488 \quad ; \quad pc = \beta_R \gamma_R E_0 \Rightarrow \quad p = 7076.751028\ eV/c$$

$$\text{Magnetic rigidity} \Rightarrow B\rho = \beta_R \gamma_R \frac{E_0}{cq} \Rightarrow B\rho = \frac{1}{0.2998} p\ [GeV/c] = 3.3355 p\ [GeV/c]$$

$$B\rho = 0.236043\ Gauss\ m \Rightarrow \text{deflection angle (earth field 0.5 gauss)}$$

$$\alpha = \frac{B_0}{B\rho} = 2.118\ rad/m = 121°/m$$

$$I = 50 - 100\ \mu Amp \quad ; \quad \text{emittance} = 173.9\ \pi\ mm\ mrad$$

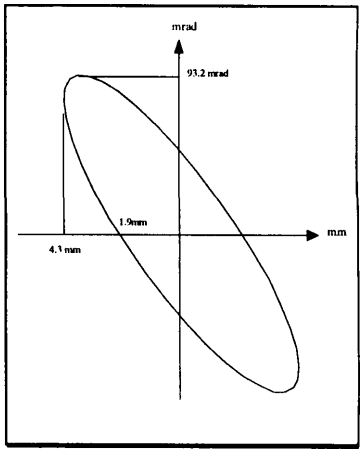

with E_0 = electron rest mass

Table 2

2	Protons	Equivalent - Electrons
Case	RFQ 2 - decelerating	RFQ 2 - decelerating
Kinetic Energy	750 keV	408 eV
Emittance tot.unorm.	30< ε <100π mm mrad	30< ε <100π mm mrad
Current	100 – 200 mA	50 – 100 μA
Energy spread	Less than 5%	Less than 5%
α Twiss	To be determined	To be determined
β Twiss (mm mrad^{-1})	To be determined	To be determined
β rel	0.03994	0.03994
γ rel	1.00080	1.00080

$$\beta_R = \left[1 - \left(1 + \frac{T}{E_0}\right)^{-2}\right]^{1/2} = 0.03993693059 \quad ; \quad \gamma_R = \frac{1}{\sqrt{1-\beta^2}} = 1.000798433217$$

$$\beta_R \gamma_R = 0.03996878694 \quad ; \quad pc = \beta_R \gamma_R E_0 \Rightarrow \quad p = 20424.0501302\ eV/c$$

$$\text{Magnetic rigidity} \Rightarrow B\rho = \beta_R \gamma_R \frac{E_0}{cq} \Rightarrow B\rho = \frac{1}{0.2998} p\,[GeV/c] = 3.3355 p\,[GeV/c]$$

$$B\rho = 0.68124252\ Gauss\ m \Rightarrow \text{deflection angle (earth field 0.5 gauss)}$$

$$\alpha = \frac{B_0}{B\rho} = 0.7339\ rad/m = 42°/m$$

$$I = 50 - 100\ \mu Amp \quad ; \quad \text{emittance} \approx 100\ \pi\ mm\ mrad$$

with E_0 = electron rest mass

Table 3

3	AntiProtons	Eq. Electrons
Case	RFQ AD- decelerating	RFQ AD - decelerating
Kinetic Energy	5300 keV	2880 eV
Emittance tot.unorm.	1,5,10π mm mrad	1,5,10π mm mrad
Current	Less than 2 mA	Less than 1μA
Energy spread	Less than 0,5%	Less than 0,5%
α Twiss	0.92	0.92
β Twiss	0.44 mm mrad^{-1}	0.44 mm mrad^{-1}
β rel	0.10613	0.10613
γ rel	1.00568	1.00568

$$\beta_R = \left[1 - \left(1 + \frac{T}{E_0}\right)^{-2}\right]^{1/2} = 0.10572338 \quad ; \quad \gamma_R = \frac{1}{\sqrt{1-\beta^2}} = 1.005636008$$

$$\beta_R \gamma_R = 0.106319238 \quad ; \quad pc = \beta_R \gamma_R E_0 \Rightarrow \quad p = 54329.13051\ eV/c$$

$$\text{Magnetic rigidity} \Rightarrow B\rho = \beta_R \gamma_R \frac{E_0}{cq} \Rightarrow B\rho = \frac{1}{0.2998} p\,[GeV/c] = 3.3355 p\,[GeV/c]$$

$$B\rho = 1.812143795\ Gauss\ m \Rightarrow \text{deflection angle (earth field 0.5 gauss)}$$

$$\alpha = \frac{B_0}{B\rho} = 0.276\ rad/m = 15°/m$$

$$I < 1\ \mu Amp \quad ; \quad \text{emittances} = 1, 5, 10\ \pi\ mm\ mrad$$

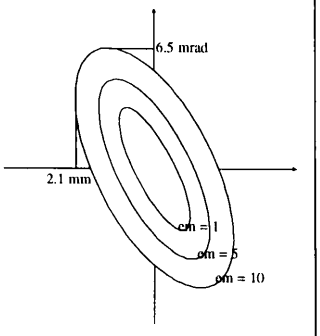

with E_0 = electron rest mass

Tables 1, 2 and 3 clearly show that the beam characteristics are quite different in the three configurations. The main difficulty lies, therefore, in creating a source as well as a transport and diagnostics line that will suit all the configurations.

1. PROPOSAL FOR THE TEST LINE

In order to have the three required electron beams with quite different characteristics, it was assumed that the experiment's general philosophy should be based on the emittance painting method. A pencil beam with variable current and little emittance has to be obtained from an electron beam. The painting consists in developing a beam steerers system enabling us to sweep it at the RFQ entrance. Furthermore, the variable current of the pencil beam allows us to model the space charge parameter appropriately, so that the equivalence between electrons and protons-antiprotons can be achieved to reconstruct the whole beam emittance in the phase space. Thus we can work in certain configurations with lower currents than those needed at the RFQ entrance.

The scheme for the realisation of the whole production and diagnostics line is shown in Fig. 1.1.

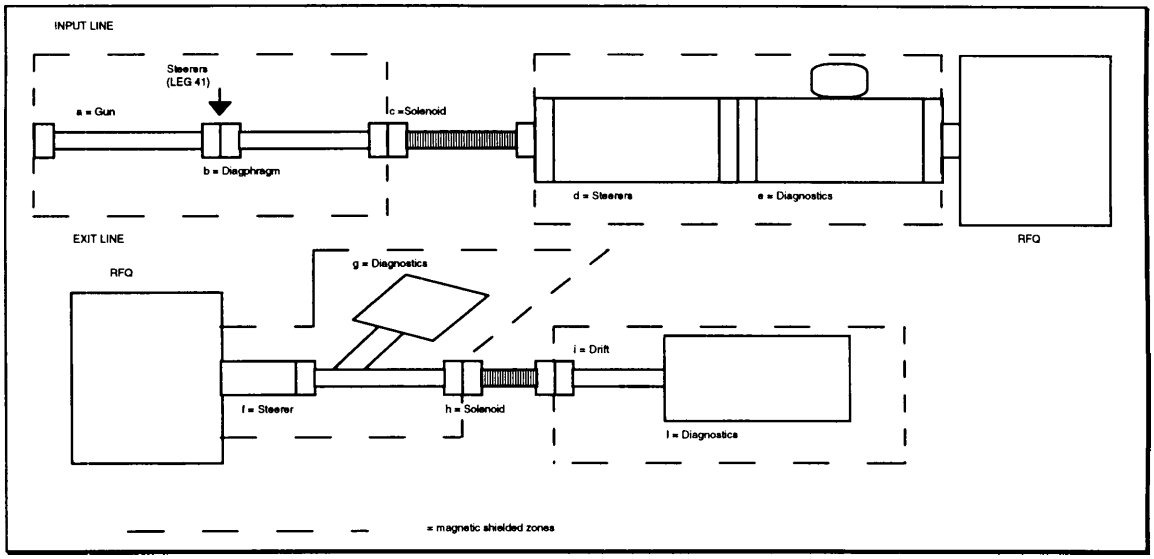

Fig. 1.1 - Line for the painting method realisation.

The beam is emitted by an electron source that is able to provide enough current at different energies (if this is not possible and if the gun has been adjusted to just one energy level a post-accelerating/decelerating system is required to reach the right current at the right energy). Once the beam has been produced in its different configurations, it can be further modelled to obtain the desired emittance for the painting by means of a two-diaphragms one-drift system. Subsequently, a focalising element (either a solenoid or an electrostatic lens) is used to direct the beam as far at the RFQ entrance. Immediately after it there is the steerers system, that is indispensable to the painting, and a diagnostics station allowing the measurement of the main beam parameters (beam size and current) at the RFQ entrance. At its exit there is another steerers system that makes it possible to reposition the pencil beam on the axis, if it needs repositioning. It can also be used as a spectrometer for an approximate energy spread measurement on the analysis line for which, once again, a diagnostics station is needed. Interestingly, most elements will be magnetically screened to avoid the effects of parasitic fields (such as the earth field), mainly for low-energy and low magnetic rigidity fields.

Let us describe the above-mentioned elements and characterise them according to our needs.

1.1 Gun (a)

We had at our disposal a RIBER CER 306 electron source, a gun that is basically used for surface analysis. The source's main scheme is shown in Fig. 1.2.

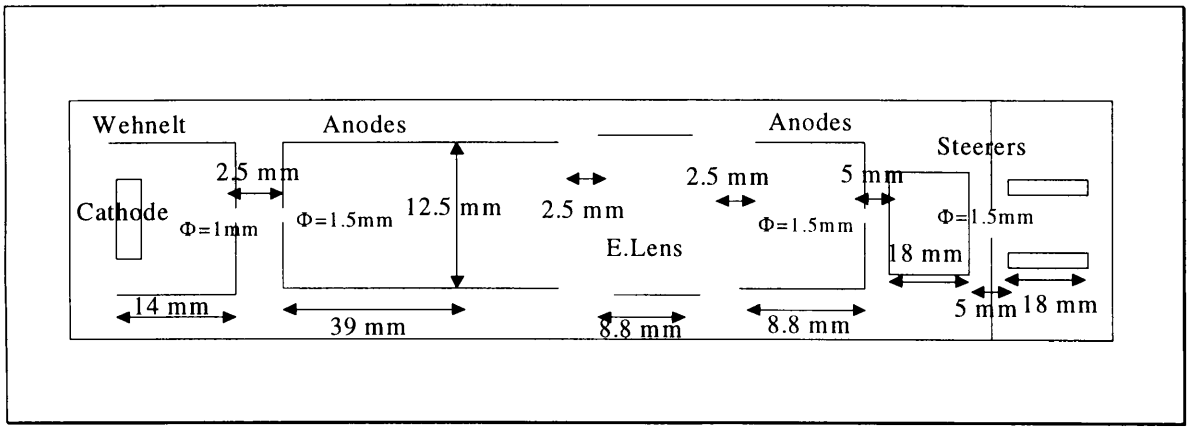

Fig. 1.2 - Scheme of the RIBER CER 306 gun structure.

The main specifications of this source are the following:

Table 4

Beam Current	Max 150 μAmp
Beam Energy	100 – 3000 eV
Filament Current	Max 3.6 A
Steerers Deflection	X = 0.42 mm Vx / keV(Energy) Y=0.48 mm Vy/KeV(Energy)

The upper limits meet our conditions (max energy = 3 kV and maximum current = about 150 μA). We still need to determine the main characteristics of the gun in the different configurations obtained by varying the anodic, Wehnelt and focalising tension and the filament current. Section 3 includes the results of the source measurements performed on a test station. The lower energy, however, is a constraint for the 49 eV configuration. Section 3 also contains the results obtained by means of diaphragms systems utilised to reduce beam energy at the gun exit.

1.2 Diaphragms system (b)

It is a system made up of two diaphragms separated by a drift. It helps select a surface in the phase space so as to carry out the desired ellipse painting at the RFQ entrance. The selection takes place as follows: the first diaphragm selects a portion of x - x' space resulting from the diaphragm size (Fig. 1.3):

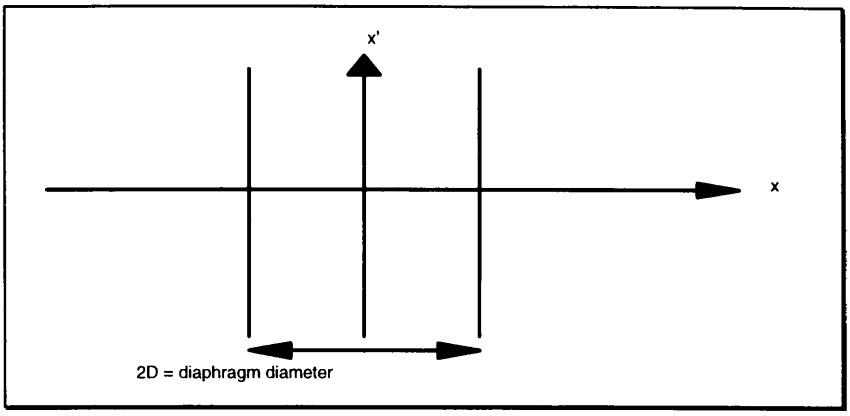

Fig. 1.3 - Effect of a diaphragm in the phase space.

Subsequently, the drift entails a linear transformation of the two lines selecting the phase space area. They make a rotation with a $1/L$ coefficient where L is the drift length. The second diaphragm finishes the selection of a finite area in the trace space (Fig. 1.4):

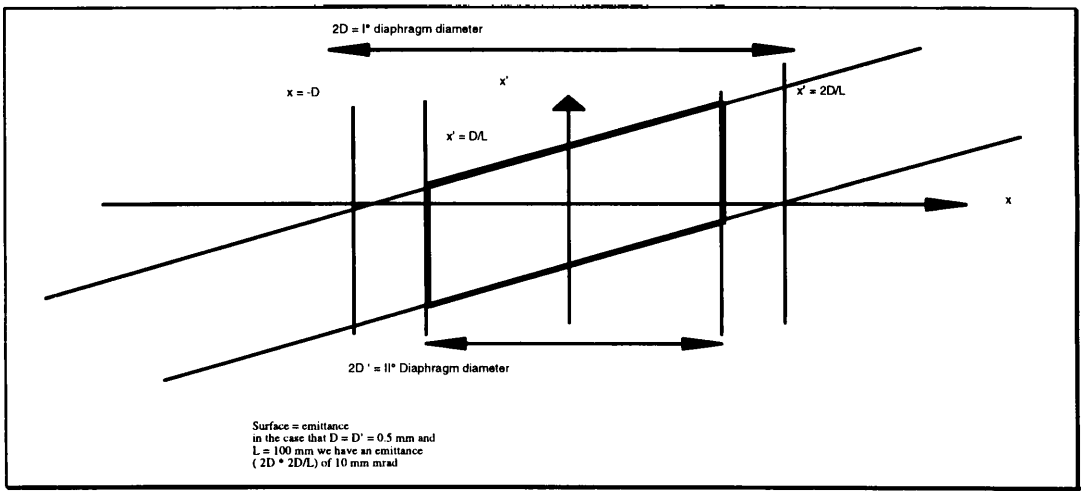

Fig. 1.4 - Effect of the system made up of two diaphragms and a drift in the phase space.

At the end, by means of the two-diaphragm system, we can obtain the small emittance beam we want that, thanks to following steerers, can be used to paint the final ellipse at the RFQ entrance. The main selection parameter will clearly be the current transmitted by the two-diaphragm system. For this reason we think it is important, in the 49 eV case, to have at our disposal a gun providing a beam which is quite collimated and with enough current at the first diaphragm's entrance.

1.3 Solenoid (c)

The solenoid following the diaphragm has the task of shaping the beam in such a way that the conditions required for painting at the RFQ entrance are met. Subsequent systems (steerers and diagnostics block) make up a drift changing the beam emittance shape significantly. In order to restore favourable conditions the use of a focalising element, like a low magnetic field solenoid or an electrostatic lens, is suggested. The line was studied by

means of simulations and numerical calculations. In fig. 1.5 we sought to simulate an ellipse inscribed into the rhomboid obtained from two identical diaphragms. Then we took an ellipse having the same x_{max} and x'_{max} as the rhomboid.

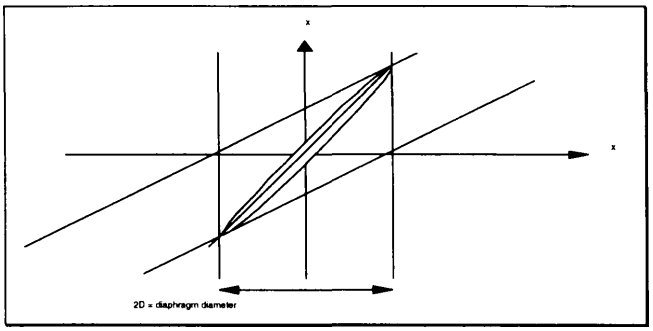

Fig. 1.5 - Emittance selected between two diaphragms and used to simulate the transport line.

We chose to make the main axis of the ellipse coincide with the rhomboid diagonal. Simulations show a minimum size for field values between 5 and 20 gauss in 49 and 408 eV configurations (see Fig. 1.6).

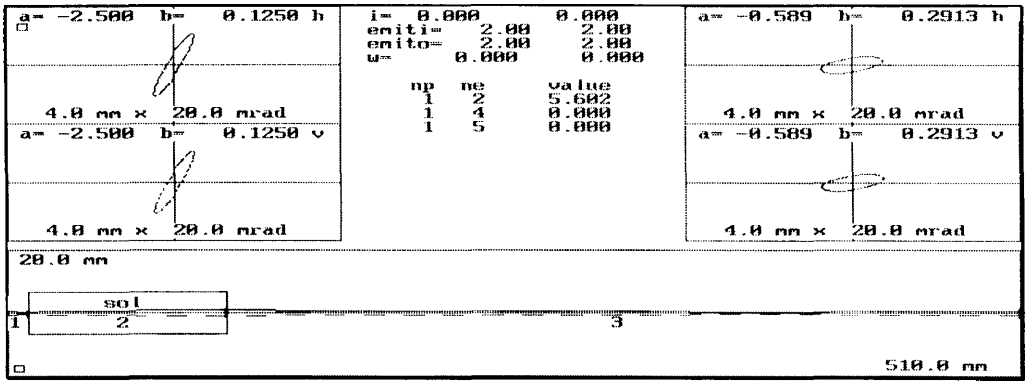

49eV

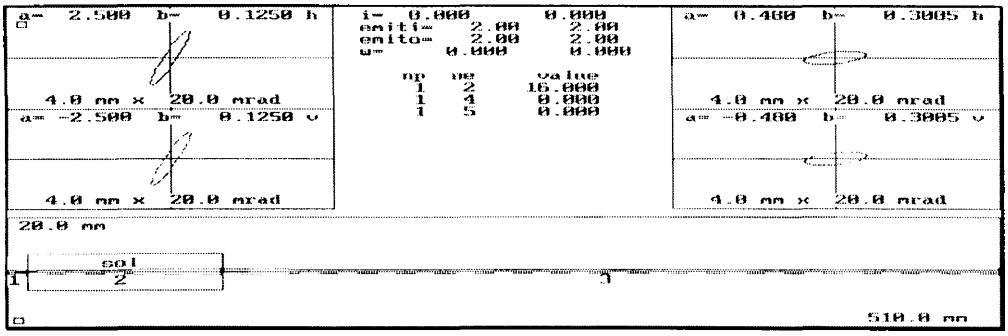

408eV

Fig. 1.6 - Beam transport simulations by means of a solenoid for 49 and 408 eV configurations.

A solenoid reaching these values (5 - 16 Gauss) is easy to manufacture using a hundred turns winding with currents varying between 0 and 2 A (see Fig. 1.7 where these solenoid fields, effective length and current were computed).

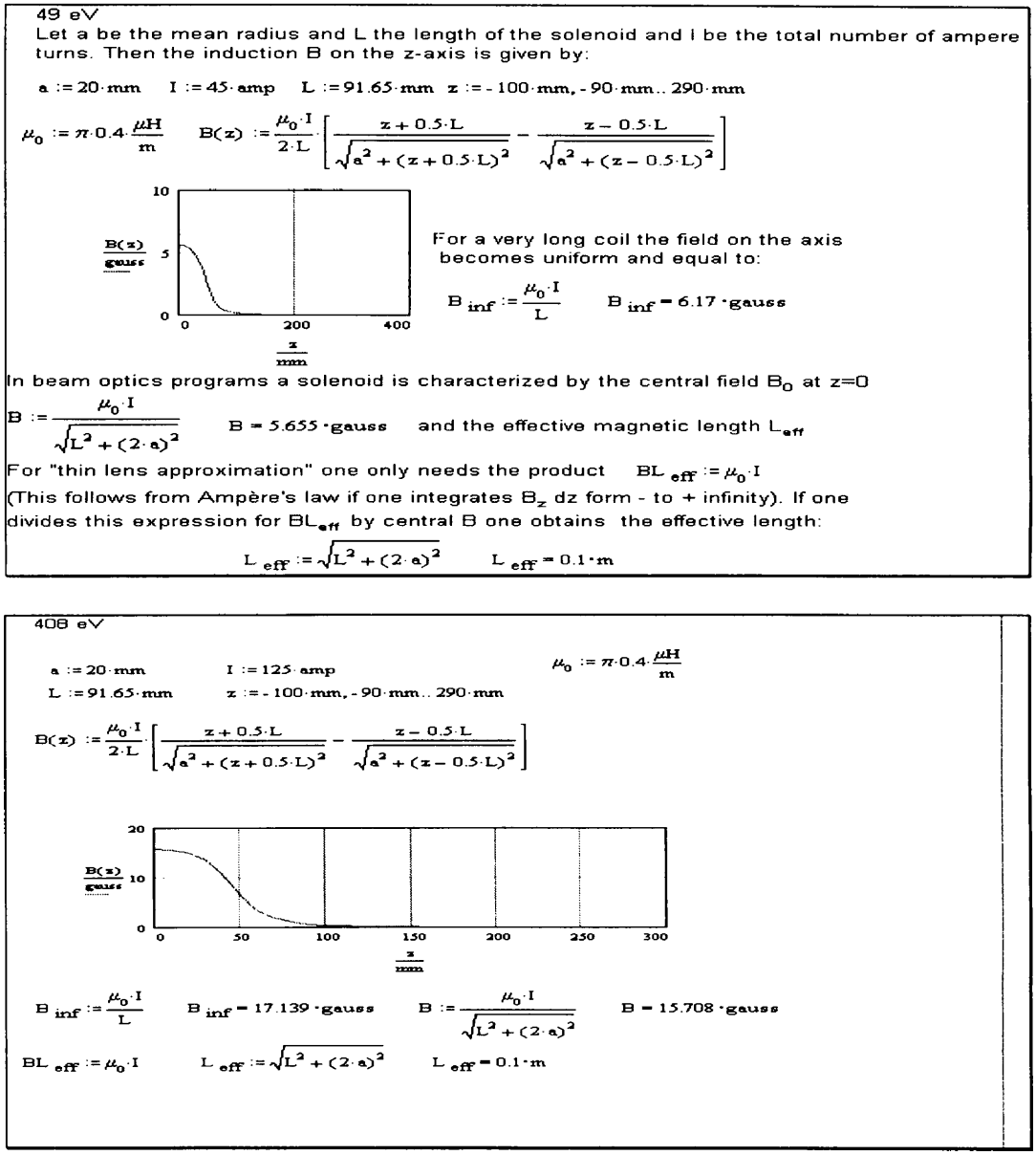

Fig. 1.7 - Field and modelling calculations of the solenoid used for 49 and 408 eV configurations.

1.3.1 Electrostatic Lens

To make the magnetic shielding of the whole line possible, it would be necessary to use electrostatic lenses instead of magnetic focalising elements. A study was therefore carried out to model an Einzel lens, using an in-house software [3] based on the matrix model described in Ref. [4]. Satisfactory results corresponding to the solenoid's behaviour were obtained in different configurations. However, as the model used is an approximation, further ray tracking analysis would be necessary.

1.4 Steerers (d)

The system we have put forward enables us to deflect the beam horizontally twice. This allows us to reach the RFQ entrance with a beam size and different inclinations so as to be able to reconstruct the emittance ellipse in 49, 408 and 2880 eV configurations.

The system is made up of two pairs of deflection plates for each size. In the suggested configuration[1], where the ratio between length and distance of the plates s/d = 0.25, we can calculate the ratio (plate tension/deflection angle by means) of the following considerations:

$$\theta = arctg\frac{Es}{p\beta} = arctg\frac{Vs}{dp\beta} \approx \frac{s}{d}\frac{V}{p\beta}, \tag{1.4.1}$$

where θ is the deflection angle, V the applied voltage, d the distance between the plates and s their length, p the particle momentum. So for unit voltage, in the three cases we have:

$$\begin{array}{ll} 49\text{ eV} & \theta = \frac{s}{d}10.2\text{ mrad} \\ 408\text{ eV} & \theta = \frac{s}{d}1.22\text{ mrad} \\ 2880\text{ eV} & \theta = \frac{s}{d}0.17\text{ mrad} \end{array} \tag{1.4.2}$$

The two geometrical parameters, s and d, have to be adjusted in such a way that we can use a signal generator with an amplifier bringing ΔV to a thousand Volts. In Fig. 1.8 we see how we can compute the maximum deflection angle and thus determine the voltage to apply to the steerers.

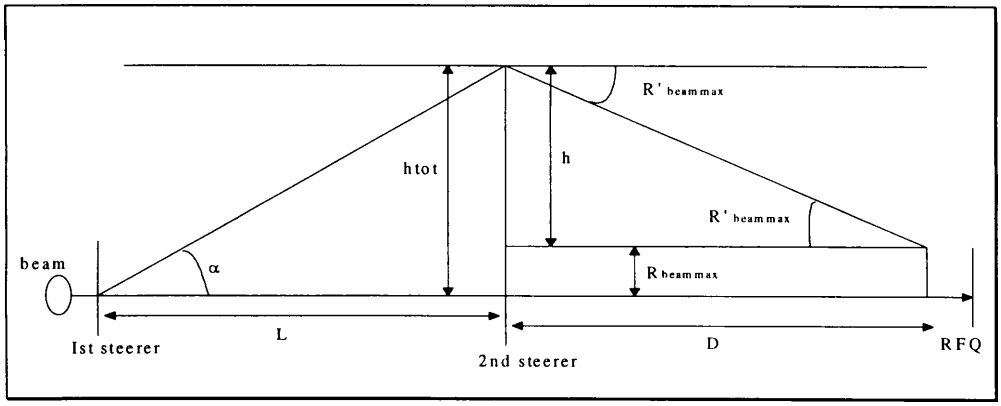

Fig. 1.8 - Scheme for the calculation of the deflection angles needed for the painting.

The beam has to be deflected by the first steerer by an angle α, and by the second by an angle $\beta = \alpha + R'_{beam\max}$ in order to be convergent at the RFQ entry, where $R'_{beam\max}$ and $R_{beam\max}$ are respectively the beam maximum divergence and size in the different configurations, L is the distance between the steerers and D is that between the last steerer and the RFQ. With easy mathematics, for little angles we obtain:

$$\beta\,[\text{mrad}] = \frac{R_{beam\max}}{L} + R'_{beam\max}\,[\text{mrad}]\left(1+\frac{D}{L}\right). \tag{1.4.3}$$

[1] See annex 1

Therefore, if the deflection n for unit voltage is known (see 1.4.2), the maximum applied voltage will be $V_{max} = \beta/n$. For instance, if we take the 2.88 keV configuration with L = 100 mm, D =300 mm, $R'_{beam\,max}$ 6.5 mrad, $R_{beam\,max}$ = 2.1 mm and n = 0.04 we obtain V_{max} ~ 730 V. Suitable software could adjust the signal sweep so as to cover the whole trace space surface under consideration, allowing the simultaneous acquisition of experimental data.

A prerequisite to define the parameters of the deflection plates making up the steerer is a linear electric field in the separation. In order to compute it, we made a number of simulations by means of POISSON (see fig. 1.9).

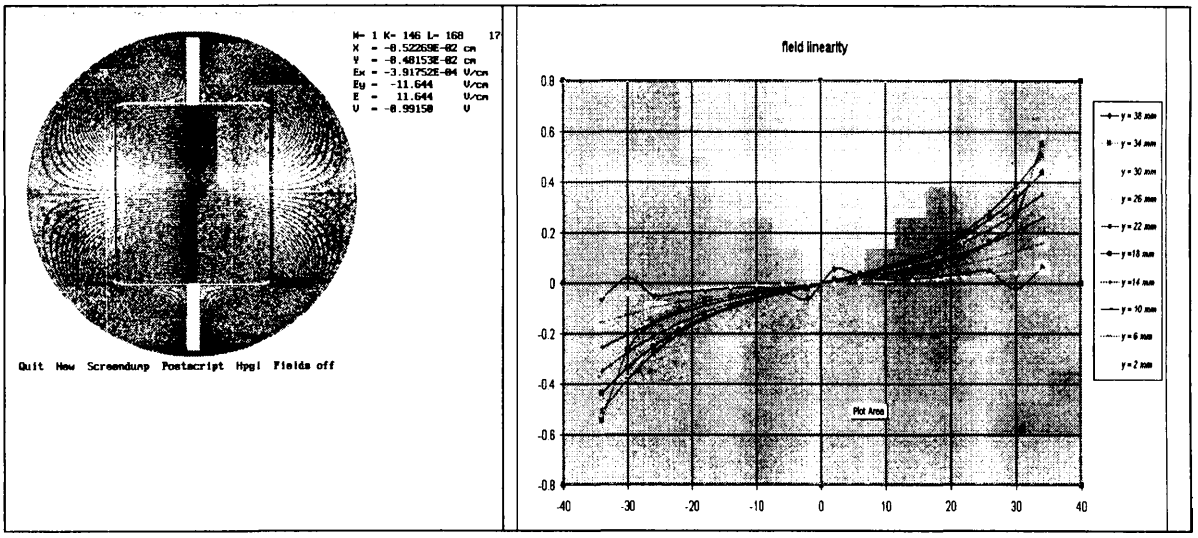

Fig. 1.9 - Simulation to compute the steerer field linearity. On the left we can see the suggested system with equipotential lines, and on the right the linearity on x as a function of different positions on y.

In an area whose side is 4 cm, linearity obtained from *Ex/Ey* ratio is maximum 16% for X = 2.0 cm. Of course, this holds true if the beam is significantly out of alignment. If the beam is perfectly aligned, the beam sides (0.5 mm) have 0.02%. This means that for a y deflection of 1 mrad the beam acquires a x of 0.0002 mrad (by all means negligible).

Bigger problems arise if the beam is significantly off axis in the second steerer. In this case it is necessary to vary the geometrical parameters to reduce field non-linearity (for example, field linearity and steerer efficiency increase, if the distance between the plates is reduced to 6.0 cm).

1.5 Diagnostics (e, g, l)

Tests and measurements of the beam characteristics require at least three diagnostic stations along the line: the first at the RFQ entry, the second at its exit and the third at the end of a spectrometer. The first and the second will enable us to analyse emittance and current before and after RFQ (therefore the transmission factor too), whereas the third will measure energy and energy spread.

As far as the first station is concerned, the essential requirement is that the total length of the diagnostics chamber should not be significant (200 - 300 mm maximum), otherwise the drift following the diaphragm would be too big; consequently, a single solenoid would not suffice to shape the beam (not to mention the magnetic field effects on such low-energy

beams). For this reason we suggest the use of a station alternatively introducing a conductive insulated plate to measure current and a fluorescent screen to measure size and position.

For the three stations we chose to use fluorescent screens for beam size and position measurements. The calculations of the photon flux emitted at a one μA incident current have enabled us to determine that in the 20 msec integration range a P47 phosphor (λ_{peak} ~ 450 nm) and a MICAM VHR 2000 CCD camera with a 16 mm-1:1.4 lens are enough to obtain a beam picture on the image plane. This configuration was successfully tested in the RIBER CER 306 gun emittance measurements. In the case of bigger object size (as for instance beam size after the spectrometer) it is possible to use a Cs(Tl) screen (λ_{peak} ~ 600 nm) to obtain a more significant photon flux.

With regard to current measurements, since at the RFQ entry the beam is continuous, we chose to utilise Faraday Cups. By polarising either the suppression ring or the plate, this enables us to carry out measurements on different energy beams, thereby purging the signal of the parasitic secondaries that could be emitted and accelerated by the RFQ. We have thus realised an in-house F. Cup model with suppression ring whose design is shown in Fig. 1.10.

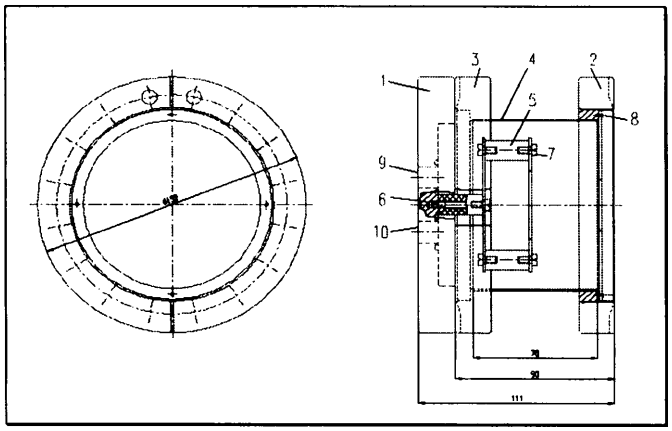

Fig. 1.10 - F.Cup design. Both the plate and the suppression ring are insulated from the vacuum chamber.

The use of variable impedances at the Faraday Cup exit allows wide-ranging current intensity measurements and signal filtering. The measurement device mainly imposes the constraint.

1.6 Steerer (f)

In order to measure the beam momentum and, therefore, its kinetic energy, at the RFQ exit we suggest the setting up of a spectrometer made up of a horizontal steerer deflecting the beam by 15° and a diagnostics station at the end. For the beam to be deflected by 15° (360 mrad) by means of an electrostatic steerer in the three configurations we can think of a higher s/d ratio. If $s/d = 0.5$ the 2880 eV beam (the most rigid) is deflected by 360 mrad at a tension of 2068 V, a range that can be attained by the HV feeders at our disposal.

1.7 Solenoid, Drift (h, i)

This small transfer line is used to carry the beam from the RFQ exit to the final diagnostics station. The features of this line may also be used for an emittance measurement

at the exit. This solenoid might have the same characteristics as the previous one for the low-energy configurations, but we suggest a reduced drift, 100 mm long.

2. THEORETICAL CONSIDERATIONS

2.1 Magnetic Shielding

Tables 1, 2 and 3 show that in the various configurations, and above all in the low-energy ones, the beam magnetic rigidity is a critical parameter. It is therefore necessary to prevent parasitic magnetic fields from influencing the beam. Moreover, the earth field may have significant consequences. Therefore, in addition to avoiding beam exposure to outside fields, the application of a magnetic shielding is required to reduce the earth field by some orders of magnitude. The method to screen the magnetic field is shielding the facility with cylinders made of a material having high magnetic permeability (mumetal, permalloy). By concentrating flux lines, the material reduces them inside the cylinder.

In approximate calculations the formulas for cylindrical geometry were used [5]. If an outside field H_0 is applied, the efficiency factor g is obtained from:

$$\boxed{g = \frac{H_0}{H_{\text{int}}} = \frac{\mu}{4}\left(1 - \frac{a^2}{b^2}\right)}, \qquad (2.1.1)$$

where H_{int} is the field inside the shielding, μ is the material permeability, a and b are the inside and outside radius of the shielding cylinder, respectively. If the thickness T is much smaller than the inside radii the formula 2.1.1 can be approximated as follows:

$$\boxed{g \approx \frac{\mu T}{2b}}. \qquad (2.1.2)$$

In our case, if we choose a material with $\mu \sim 20{,}000$ (for weak fields), a thickness of 0.2 mm and a diameter of 100 mm, g equals 40. To increase efficiency, another μ metal cylinder can be added. An approximate analytical model provides the efficiency for a two-layer system [6]:

$$\boxed{g \approx g_1 + g_2 + g_1 g_2 \left(1 - \left(\frac{b_1}{b_2}\right)^2\right) = g_1 + g_2 + g_1 g_2 J}. \qquad (2.1.3)$$

By the suffixes 1 and 2 we mean the inside and outside layer, respectively[2].

For example let us name g_1 the efficency of the above-mentioned cylinder ($g_1 = 40$) and g_2 the efficency of another cylinder made of the same material, having the same thickness but whose diameter is twice that of the first one (so $g_2 = 20$). So we have:

$$\boxed{g = g_1 + g_2 + g_1 g_2 J = 60 + 800J = 60 + 800(0.75) = 660}$$

[2] In many reference books, in the case of a double cylinder the result $g = g_1 g_2$ is given, thus neglecting the J factor that takes into account the interaction of the two cylinders. Of course, this is wrong, and can lead to remarkable discrepancies with the theory.

If the outside field is not just the earth field, but a higher intensity one, we should be careful not to exceed saturation level (or even hysteresis curve knee) that in the case of mumetal can be in the 0.4-0.8 Tesla range. To compute the field inside the material the following formula can be applied [5]:

$$\boxed{B(\,gauss\,) \approx \frac{2.5bH_0}{T}}. \qquad (2.1.4)$$

For a 0.2 thick sheet with a diameter of 100 mm and an applied field of 0.5 gauss (earth field) the field inside the material is of 312.5 gauss, therefore below saturation level. However, we should be careful because the equation (2.1.4) shows that the outside field leading to hysteresis curve knee inside the material (0.5 T) is 8 Gauss. If the intensity of the applied field is higher, a preliminary field shielding by means of a soft iron sheet is recommended where the saturation value is higher (~ 1.5 T).

To confirm the validity of the applied model a number of simulations were performed with POISSON and MAFIA 2D & 3D codes. Let us present the results and compare them with the ones obtained from the model:

Table 5

Case	*Inner radius*	*Inner thickness*	*Inner μ*	*Outer radius*	*Outer thickness*	*Outer μ*	*Cylinders length*	*Total g*
Theory model	*36.9 mm*	*0.9 mm*	*20000*	*50 mm*	*3 mm*	*200*	*∞*	*~ 900*
Poisson 2D	*36.9 mm*	*0.9 mm*	*20000*	*50 mm*	*3 mm*	*200*	*∞*	*~ 658*
Mafia 2D	*36.9 mm*	*0.9 mm*	*20000*	*50 mm*	*3 mm*	*200*	*∞*	*~ 707*
Mafia 3D	*36.9 mm*	*0.9 mm*	*20000*	*50 mm*	*3 mm*	*200*	*250 mm*	*~ 608*

The simulations agree, but they differ from the approximate analytical model by a 30% factor.

2.2. Vacuum requirements

The low energy of the electron beams under consideration entails low magnetic rigidity and consequently justifies the use of a magnetic shielding. However, this is not the only aspect to consider as far as non-relativistic beams are concerned. Vacuum chamber residual gases can have remarkable effects on the dynamics of the beams in question. The following paragraph illustrates the calculations performed to assess the emittance increase due to the elastic scattering of electrons with residual gas as well as the energy loss due to collisions. Both effects set upper limits on vacuum chambers pressure.

2.2.1 Multiple scattering

Let us start with the scattering of a particle from another particle. Particle 1, moving at uniform velocity v, collides with particle 2 with impact parameter b. The momentum spread is given by [7]:

$$\boxed{\Delta p = \frac{2\,Z_1 Z_2 e^2}{vb}} \tag{2.2.1}$$

with $Z_1 e$ = charge of the first particle and $Z_2 e$ charge of the second one. Therefore:

$$\boxed{\theta = \frac{\Delta p}{p} = \frac{2\,Z_1 Z_2 e^2}{vbp} \Rightarrow \frac{d\sigma}{d\Omega} = b\frac{db}{\theta\, d\theta} = \left(\frac{2\,Z_1 Z_2 e^2}{vp}\right)^2 \frac{1}{\theta^4}}. \tag{2.2.2}$$

If the Fermi-Thomas potential function [7] is taken into account, we can fix an upper and a lower limit for the angular variable with regard to power behaviour. It follows that:

$$\boxed{\langle\theta\rangle^2 = \frac{\int \theta^2 (d\sigma/d\Omega) d\Omega}{\int (d\sigma/d\Omega) d\Omega} = 2\theta_{\min}^2 \; ln\left(\frac{\theta_{\max}}{\theta_{\min}}\right) = 4\theta_{\min}^2 \; ln\left(204 Z_g^{-1/3}\right)}, \tag{2.2.3}$$

where the deflection of electrons (Z = 1) from an atom (Z_g) has been considered. Let us consider an electron crossing a T thick medium with N atoms per volume unit. After a high number of n bumps, statistic independence enables us to approximate angular distribution to a Gaussian, centred on the incidence direction, with mean square angle:

$$\boxed{\langle\Theta\rangle^2 = n\langle\theta\rangle^2 = 4\pi N\left(\frac{2Z_g e^2}{pv}\right)^2 ln\left(204 Z_g^{-1/3}\right) T}. \tag{2.2.4}$$

Following the procedure described in Ref. [8], the increase per metre of the unnormalised rms emittance is obtained:

$$\boxed{\frac{d\varepsilon}{ds} = 7\cdot 10^{-6}\,\beta_T P\,(\text{Torr})\left(\frac{Z_g}{\beta^2\gamma}\right)^2 ln\left(204 Z_g^{-1/3}\right)}, \tag{2.2.5}$$

with β_r = Twiss parameter, $\beta = v/c$. If we take into account oxygen (Z = 8), β_T = 0.1 and 50 eV (β = 0.013), we see that:

$$\frac{d\varepsilon}{ds}(\text{ mrad/m }) \sim 10^4\, P\,(\text{Torr})$$

This means that for emittance to increase by 1mm mrad/m a 10^{-10} P (Torr) vacuum level is needed!

Warning: These formulas hold true for elastic scattering; it means that we assume that deviation is much bigger than energy loss. This model cannot be applied to very low energies for small parameter impacts (big θ_{max}) because energy loss has to be considered too (the effect can be a flattening of the scattering angle). In any case, the pressure value needed to avoid emittance growth is still very low.

2.2.2 *Energy loss*

The Bethe Block formula corrected for electrons is [9]:

$$\frac{d\varepsilon}{ds} = \left(\frac{r_e}{\beta}\right)^2 2\pi Z_g E_0 n_g \left[ln\left(\frac{T\beta^2\gamma^2 E_0}{2I^2}\right) + \frac{1}{\gamma^2} - \left(\frac{2}{\gamma} - \frac{1}{\gamma^2}\right) ln\,2 + 0.125\left(1 - \frac{1}{\gamma}\right)^2 \right] \quad (2.2.6)$$

where r_e = electron radius, Z = oxygen, N_g = oxygen density, E_0 = electron rest energy, T = electron kinetic energy, I = ionisation potential (~10Z). In our case, with a 10^{-6} mbar pressure at 300K for a tube whose section is 10 cm^2 , energy loss is ~30 eV/m.

3. GUN RIBER CER 306 – SOURCE CHARACTERISATION

After our line proposal and some theoretical considerations, we now wish to present the results obtained in the electron source characterisation at our disposal, that is the RIBER CER 306 gun. To determine its characteristics we measured the emitted beam current as a function of the voltages and currents applied and we assessed its dynamic quality by means of emittance measurement. To this end, we set up a test station. The connections for the gun's power supply are shown in Annex 2. The line was therefore made up of the source and a diagnostics station equipped with a Faraday Cup for current measurements and a fluorescent screen for beam size measurements.

3.1 Current measurements

In the RIBER CER 306 gun specifications the energy range is said to be 100 - 3000 keV. A number of different current measurements were carried out in the 2880, 2000, 1880, 1000 and 408 eV configurations. At higher energies the best gun performances were obtained. Let us present the results of the 2880 and 2000 eV measurements made by alternatively varying the extraction grid (wehnelt) tension and the filament current:

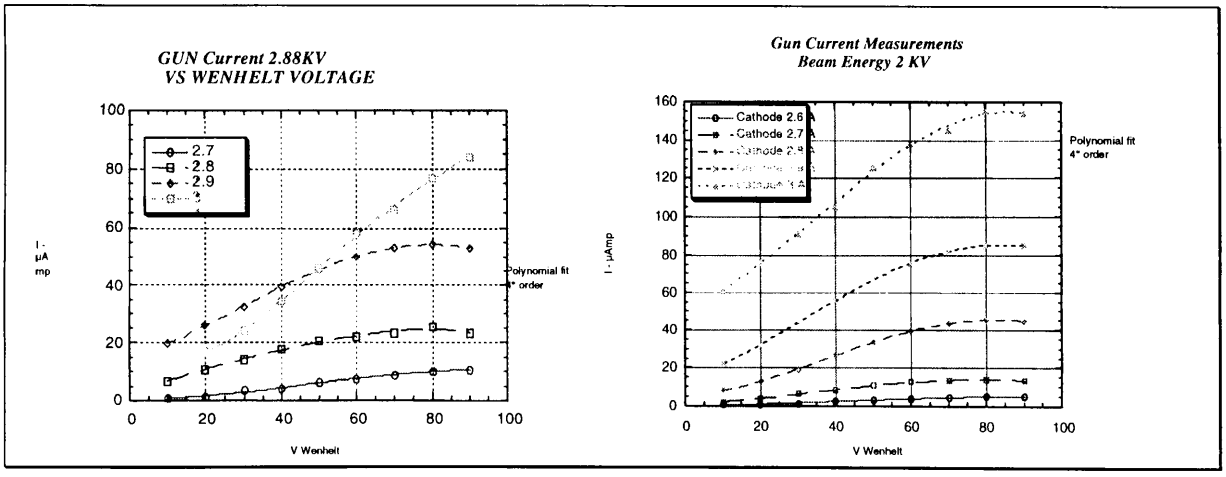

Fig. 3.1 - Current measurements for 2 and 2.88 keV energy beams

The relationship between the emitted current and the wehnelt tension changes if energy is reduced. Practically the tension value corresponding to the maximum emitted current decreases, as can be seen in the 1000 eV measurement with cathode current = 3 A (Fig. 3.2).

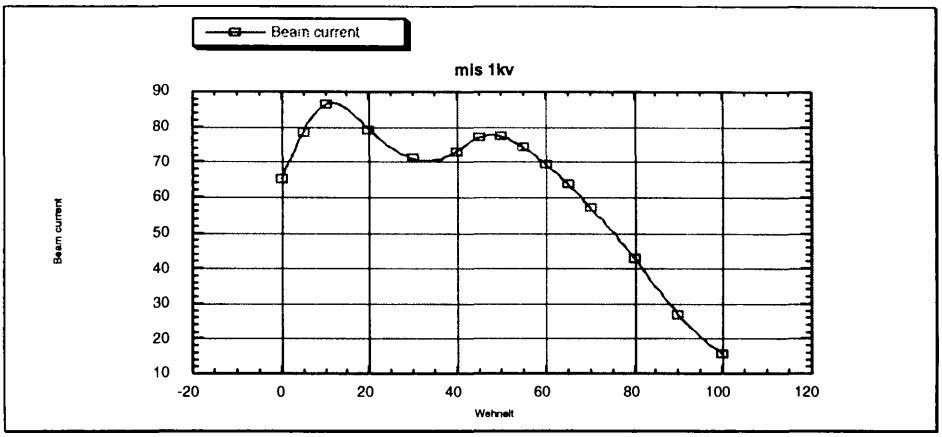

Fig. 3.2 - 1 keV beam current measurement.

The optimised 408 eV tension values resulted in a maximum emitted current of about 50 μA. No current was noted in the 49 eV configuration. The current, in fact, plummets below 100 eV. This is matched by an increase in emittance and, consequently, in beam size. So the beam is not properly transported along the analysis line. To highlight the effects on the beam of the energy increase and change, another two measurements were performed (Fig. 3.3). The former reveals beam size as a function of filament current (for a 2 keV beam). Interestingly, the charge effect makes beam size increase until it explodes. The latter measures beam size as a function of its energy, when the focalisation tension is optimised for 2 keV. It is therefore possible to highlight the focalising force dependence on energy. The beam size measurement images were acquired by means of an in-house software [10] on Unix platform.

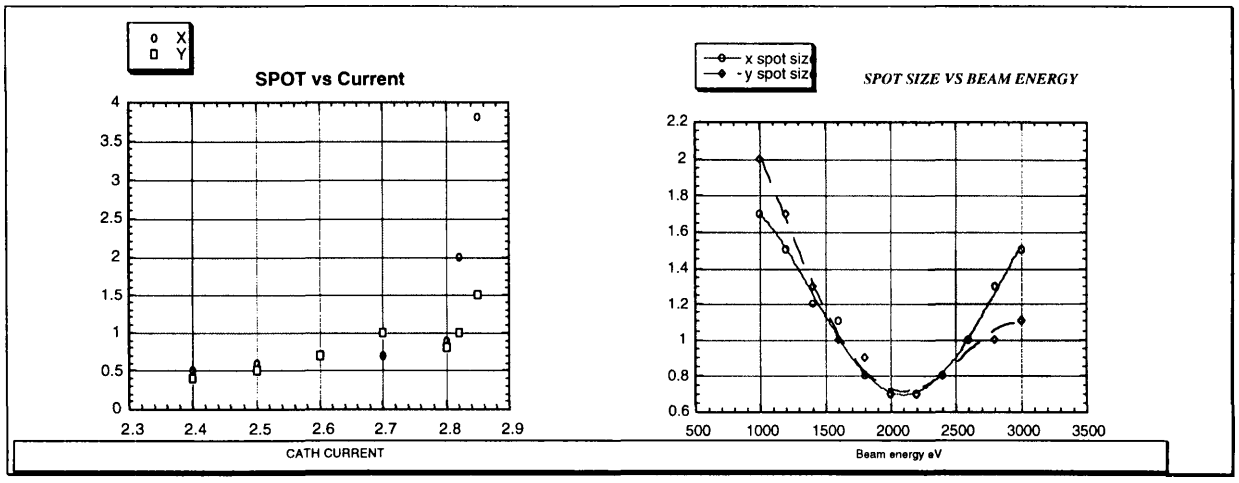

Fig. 3.3 —Beam spot size measurements vs cathode current and beam energy. Beam diameter is expressed in mm.

Since in the 49 eV configuration a beam emission was not obtained, the attempt was made to change gun set-up (Fig. 3.4). A decelerating diaphragm was then added after the

source so that varying anodic tension against that of the earthed diaphragm could attain the right energy.

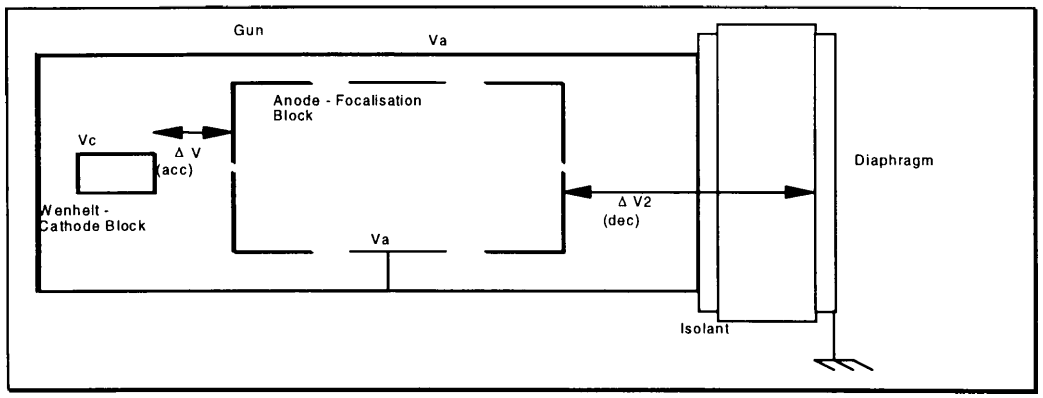

Fig. 3.4 - Source set-up with decelerating diaphragm to obtain a low-energy beam (~50 eV).

We therefore tried to measure the current coming out of the diaphragm by placing the Faraday Cup immediately after it. Moreover, given the high beam divergence at the exit, we decided to measure the current on the Faraday Cup vacuum chamber: our aim was to understand what is the overall current truly emitted by the diaphragm without the constraint placed by the opening angle given by the Faraday Cup plate. The optimised set results were about 10-15 μA on the chamber and 5-6 μA on the plate. Since the factor is already significant on beam divergence at the exit, the test was repeated, this time inserting the two-diaphragm system for emittance selection. This measurement gave no results on the Faraday Cup: it is therefore evident that owing to the high emittance and vacuum scattering effects (in our set the value is ~ 10^{-6} mbar), the beam is completely scattered along the diaphragms line.

So it seems that the gun is not suitable for the 49 eV low energy configuration. Only in the set where the gun was close to the Faraday Cup did we obtain a current that can be measured at the above-mentioned energy. As far as realistic solutions are concerned, a gun suitable for low-energy, high-current emission could be bought. For this purpose, the VG LEG 63 and LEG 41 models were studied. The former has a 0.1-5 kV range, therefore a low-energy deceleration is required, anyway. The latter, instead, is designed to provide significant currents at low-energy; consequently it does not need any adjustment to provide a 49 eV beam. The problem with the LEG 41 model is the lack of a beam deflection system which makes it necessary to add both vertical and horizontal steerers. The required tension would not exceed 100 V. Of course, higher energy configurations could be made with available RIBER CER 306 gun.

3.2 Emittance measurements

To complete the dynamic characterisation of the source we performed a beam emittance measurement at 1.88 keV energy. To this end, we adopted the statistical approach and applied it to the three gradient method [11]. We built a transfer line with some drifts and a focalising element (a solenoid). We injected the beam and varied the solenoid strength by 10 different values. For each of them the R transport matrix was computed by means of the TRACE software, and three images were acquired so as to obtain the rms beam size and its related error (corrected by the camera resolution). At this point, the MINUIT software allowed us to minimise the CHI-SQUARE function defined as follows:

$$\chi^2 = \sum \frac{(f_{mes} - f_{teo})}{\sigma^2}$$

where f_{mes} = measurements ; $f_{teo} = R\sigma ij$

with σij = beam matrix and R = Transport matrix. (3.2.1

Here are the measurement results:

Table 6

Type	$X\ 4\sigma$	$Y\ 4\sigma$
Emittance unorm. (mm mrad)	1.17	1.36
X_{max} (mm)	0.56	0.59
r_{12}	- 0.65	-0.59
x'_{max} (mrad)	11.0	11.37

Discrepancies between the horizontal and vertical size can be explained by the imperfect alignment between the beam and the solenoid (we noted a little displacement during the solenoid field variation).

CONCLUSIONS

The study may be summarised in a few considerations. Most technical details and physical aspects were taken into account; we can therefore draw the following conclusions: the envisaged electron beam tests are feasible, at least in the 2.88 keV configuration, provided attention is paid to the constraints imposed by parasitic magnetic fields and residual gases scattering calculations. Results show that the available source is by no means suitable for low-energy measurements for which another source should be considered, right from the beginning. In any case the constraints placed by low energies can hardly be bypassed in RFQ 2 (where vacuum is $\sim 10^{-7}$ mbar and the tank is magnetised). Therefore, the proof of principle ought to be carried out on another radio frequency device. The study proves, however, the experiment feasibility in the RFQ AD configuration.

ANNEX 1

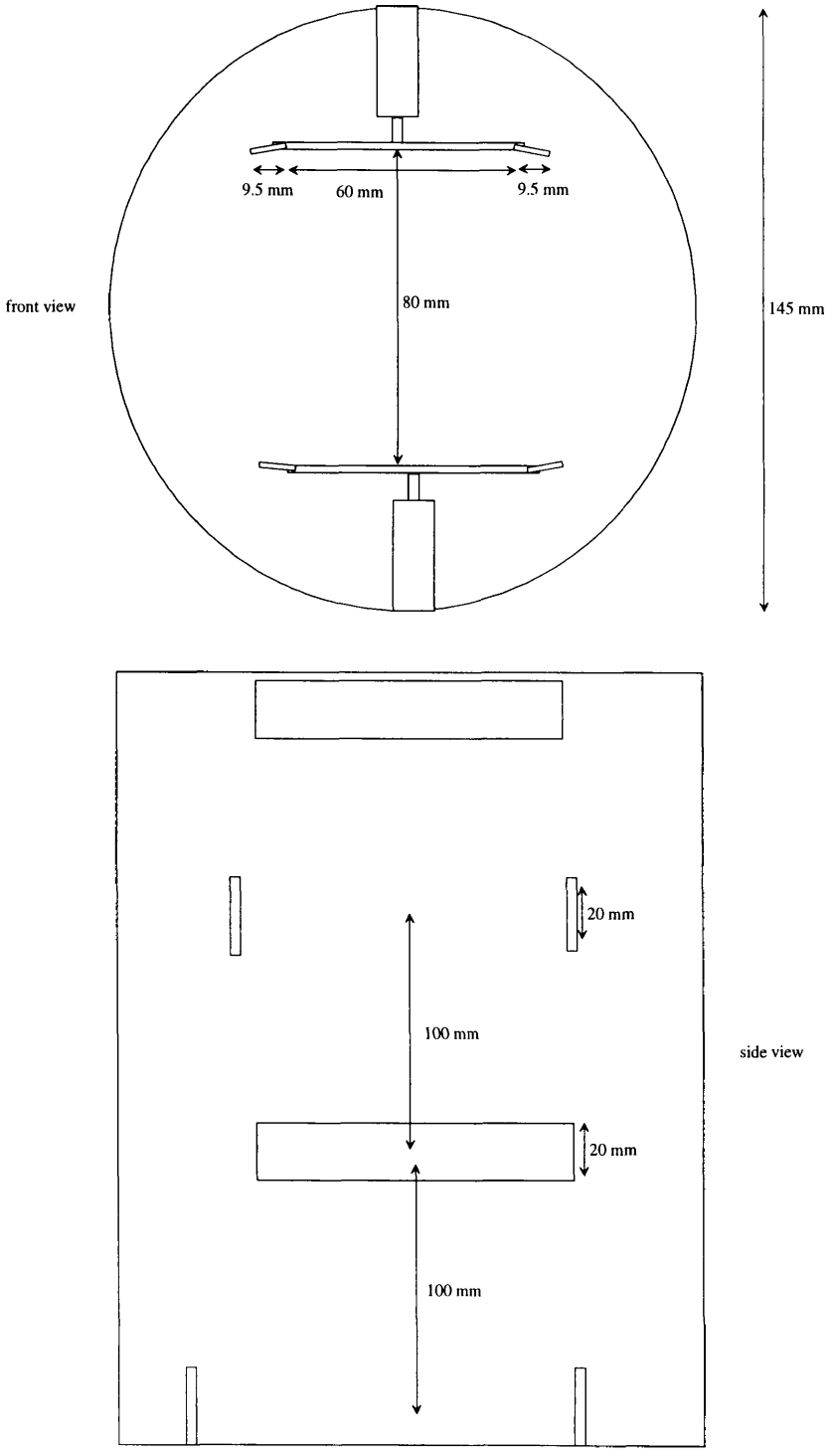

Proposal for the steerer system realisation.

ANNEX 2

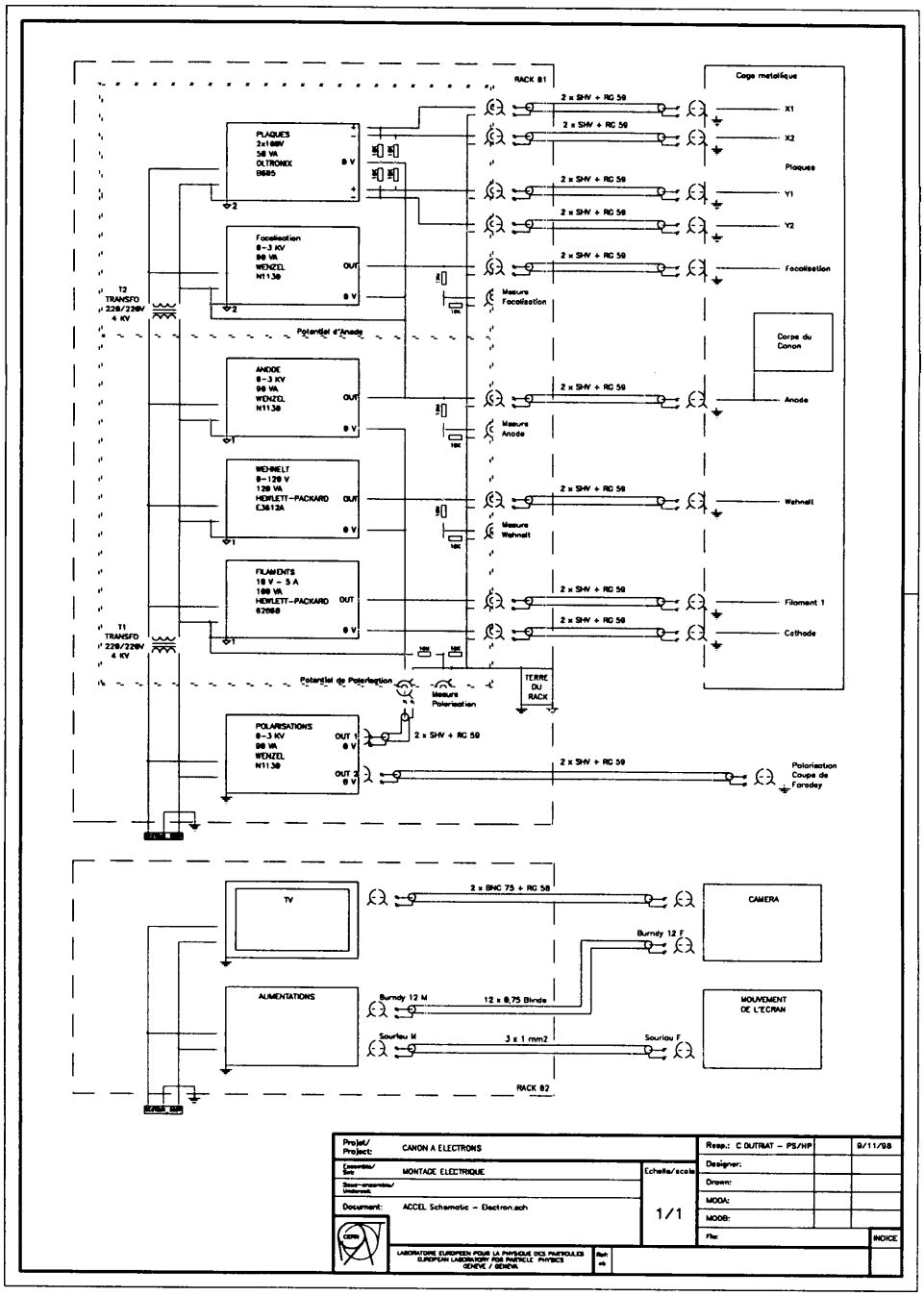

Electrical scheme of the connection between the power supply and the RIBER CER 306 electron gun

REFERENCES

1] J. Bosser et al.: *"Feasibility Study of a Decelerating Radio Frequency Quadrupole System for the Antiproton Decelerator AD"*, PS/HP Note 97-36, Editor W.Pirkl, 1997.

2] E. Tanke, M. Vretenar, M. Weiss: *"Measurements of the CERN High Intensity RFQ"*, EPAC Proceedings 1992, p. 542.

3] R. Tracz: Private Communication.

4] J.Q. Lu, I. Ben-Zvi and J.Cramer: *"LYRAN. A Program for the Analysis of Linac Beam Dynamics"*, N.I.M Phys.Res. A 262, 200-6, 1986

5] *Reference Catalogue of the Mμshield Company.*

6] E. Dahlberg: *"Electromagnetic Shielding, Some Simple Formulae for Closed Uniform Shields"*, TRITA –EEP 75-27, Dpt of Plasma Physics, Royal Institute of Technology, Stockholm (Sweden), 1975.

7] J.D. Jackson: *"Classical Electrodynamics"*, J. Wiley & Sons, Second Edition, New York 1975.

8] M. Reiser: *"Theory and Design of Charged Particle Beams"*, J. Wiley & Sons, New York 1994.

9] K.S. Krane: *"Introductory Nuclear Physics"*, J. Wiley & Sons, New York 1988.

10] U. Raich: Private Communication

11] A.Variola: *"Utilisation du Rayonnement Optique pour l'Etude des Caracteristiques Spatiotemporelles d'un Faisceau d'Electrons. Application à TTF"*, Thèse de doctorat, Université de Paris Sud, LAL 98-01, Paris 1998